

Multi-omics profiling identifies C1QA/B⁺ macrophages with multiple immune checkpoints associated with esophageal squamous cell carcinoma (ESCC) liver metastasis

Fei Zheng, Wei Zhang, Baihua Yang, Mingqiu Chen

Department of Radiation Oncology, Clinical Oncology School of Fujian Medical University, Fujian Cancer Hospital, Fuzhou, China

Contributions: (I) Conception and design: M Chen; (II) Administrative support: M Chen; (III) Provision of study materials or patients: F Zheng; (IV) Collection and assembly of data: W Zhang; (V) Data analysis and interpretation: B Yang; (VI) Manuscript writing: All authors; (VII) Final approval of manuscript: All authors.

Correspondence to: Mingqiu Chen. Department of Radiation Oncology, Clinical Oncology School of Fujian Medical University, Fujian Cancer Hospital, Fuzhou 350014, China. Email: drchenmingqiu@163.com.

Background: Esophageal squamous cell carcinoma (ESCC) is a highly lethal malignant tumor lacking effective treatments; 20% of ESCC patients develop liver metastasis with an extremely short survival time of ≈ 5 months. The tumor microenvironment (TME) plays a crucial role in tumor homeostasis, but the relationship between the ESCC TME and liver metastasis is still unknown.

Methods: To identify potential cell populations contributing to ESCC liver metastasis, single-cell RNA (scRNA) sequencing data were analyzed to identify the major cell populations within the TME. Each of the major cell populations was re-clustered to define detailed cell subsets. Thereafter, the gene set variation analysis (GSVA) score was calculated for the bulk RNA-seq data based on the gene signatures of each cell subset. The relationship between the GSVA score of each cellular subset and clinical outcome was further analyzed to identify the cellular subset associated with ESCC liver metastasis, which was validated by multiplex immunohistochemistry.

Results: C1QA/B⁺ tumor-associated macrophages (TAMs) acted as the central regulator of the ESCC TME, closely associated with several key cell subsets. Several immune checkpoints, including CD40, CD47 and LGALS9, were all positively expressed in C1QA/B⁺ macrophages, which may exert central regulatory control of immune evasion by ESCC via these immune checkpoints expressions.

Conclusions: Our results comprehensively revealed the landscape of tumor-infiltrating immune cells associated with ESCC prognosis and metastasis, and suggest a novel strategy for developing immunotherapies for ESCC liver metastasis by targeting C1QA/B⁺ TAMs.

Keywords: Esophageal squamous cell carcinoma (ESCC); C1QA/B⁺ tumor-associated macrophages (C1QA/B⁺ TAMs); multi-omics profiling

Submitted Oct 18, 2022. Accepted for publication Nov 23, 2022.

doi: 10.21037/atm-22-5351

View this article at: <https://dx.doi.org/10.21037/atm-22-5351>

Introduction

Esophageal cancer is one of the most serious diseases threatening human health (1) and esophageal squamous cell carcinoma (ESCC) is the predominant histological type, accounting for $\approx 90\%$ of esophageal cancers worldwide (2). The etiology of ESCC mainly comprises of cigarette

smoking, alcohol drinking, hot food and beverages, pickled vegetables, radiation damage, and genetic factors (3). Generally, ESCC is diagnosed at an advanced stage due to the low sensitivity and efficiency of endoscopy and barium swallow techniques (4). The 5-year overall survival (OS) rates of ESCC are $<20\%$, due to tumor recurrence,

extensive invasion and metastasis (5). The liver is the major distal metastasis site of ESCC and ≈20% of ESCC patients develop liver metastasis.

Extraordinary advances have been made in the diagnosis and treatment of ESCC. PD-1 antibodies such as pembrolizumab and nivolumab have been used in clinical trials to treat patients with advanced ESCC (6), but the prognosis of ESCC remained poor, and only subtle improvement was achieved in OS compared with traditional chemotherapy (7); for the liver metastasis patients especially, the median survival time is only 5 months. Therefore, the tumor microenvironment (TME) of ESCC to profile the immune status for elucidation the mechanism of ESCC liver metastasis, and development of innovative immunotherapies for ESCC.

Single-cell RNA sequencing (scRNA-seq) is widely utilized for analysis of the heterogeneity of complex biological systems (8). Currently, single-cell transcriptomic analysis provides a strategy for synthetically elucidating intercellular relationships in complex TMEs (9). The types and status of tumor-infiltrating immune cells have been well distinguished and dissected by scRNA-seq in lung cancer (10), hepatocellular carcinoma (11) and breast cancer (12). In this study, high-dimensional scRNA-seq obtained from a Gene Expression Omnibus (GEO) dataset combined with an RNA-Seq dataset were used to describe the immune landscape of ESCC. Furthermore, we identified gene signatures by gene set variation analysis (GSVA) score to explore the relationship between specific cell subsets and survival probability.

Briefly, major cell populations such as B and T lymphocytes, granulocytes, natural killer (NK) cells and macrophage (MΦ) were clustered and redefined. We found

several unique cell subsets correlated to patient prognosis and liver metastasis, and the C1QA/B⁺ tumor-associated macrophages (TAMs) were likely to be the central regulator in the ESCC TME. Furthermore, analysis indicated that the key molecules in immune regulation included TNFSF9, CD40, and CD47, mediated by the C1QA/B⁺ TAMs. Therefore, our results comprehensively revealed the landscape of tumor-infiltrating immune cells associated with ESCC prognosis and metastasis, and provided a novel strategy for developing immunotherapies for ESCC liver metastasis targeting C1QA/B⁺ TAMs. We present the following article in accordance with the MDAR reporting checklist (available at <https://atm.amegroups.com/article/view/10.21037/atm-22-5351/rc>).

Methods

scRNA-seq data analysis

Raw sequencing data were preprocessed by Cell Ranger 3.0.1, then unique molecular identifier (UMI) count data were generated by inputting the fastq files into the Cellranger count. Single-cell data analysis was conducted using R package Seurat (<http://satijalab.org/seurat>) (13). Briefly, high-quality cells (>200 genes and <6,000 genes/cell, <10% mitochondrial genes) were kept for downstream analysis. Datasets were integrated using the Seurat package to eliminate batch effects, followed by principal component analysis, and Uniform Manifold Approximation and Projection (UMAP) visualization. Graph-based clustering was applied to identify clusters using default parameters.

The Cancer Genome Atlas (TCGA) data analysis

ESCC RNAseq data were downloaded from TCGA database, accompanied by corresponding clinical information. GSVA was performed based on the cluster-specific gene sets derived from scRNA-seq to assign cell type signature scores per sample ranging from -1 to +1 (14).

Multiplex immunohistochemistry (mIHC) assay

Tissues samples were obtained from the patients with ESCC liver metastasis from Fujian Cancer Hospital between January 2018 to August 2020. The study was conducted in accordance with the Declaration of Helsinki (as revised in 2013). The study was approved by the ethics committee of Fujian Cancer Hospital (No. 10104700) and informed

Highlight box

Key findings

- C1QA/B⁺ tumor-associated macrophages (TAMs) acted as the central regulator of the esophageal squamous cell carcinoma (ESCC) liver metastasis.

What is known and what is new?

- The tumor microenvironment (TME) plays a crucial role in tumor homeostasis;
- C1QA/B⁺ TAMs acted as the central regulator of the ESCC TME.

What is the implication, and what should change now?

- A novel strategy for developing immunotherapies for ESCC liver metastasis by targeting C1QA/B⁺ TAMs.

consent was taken from all individual participants. Multiplex staining of primary ESCC tissues and their corresponding liver metastasis was performed using Opal™ 7-color multiplex IHC kit (Akoya Biosciences, NEL861001KT, USA) according to the manufacturer's instructions (15). Briefly, the slides were incubated for approximately 1 h at 68 °C followed by deparaffinization and rehydration. For each staining cycle, the slides were treated with retrieval of antigen, blocking, and primary antibodies incubation, followed by horseradish peroxidase-conjugated secondary antibody incubation and Opal tyramide signal generation (detailed information of antibodies and corresponding Opal fluorophores are given in Table S1). The slides were stripped with retrieval solution as required before the next round of staining. The above process was repeated until all markers were completed. Once all markers were labeled, slides were counterstained with DAPI (Akoya Biosciences) and scanned using the PerkinElmer Vectra3® Polaris™ platform. The multispectral images obtained were unmixed using the inForm Advanced Image Analysis software (inForm 2.4.1; Akoya Biosciences). The antibodies and reagents are listed in Table S1.

Statistical analysis

Kaplan-Meier survival plots were generated by survival and survminer package in R. The log-rank test was used to calculate the statistical significance between the survival curves. $P < 0.05$ was considered significant. No data point was excluded from analysis. No blinding or randomisation was performed for statistical analysis. Sample size was determined to ensure the proper comparison between different groups.

Results

Experimental scheme and single-cell transcriptomic landscape of ESCC

To clarify the potential effect of different cell subpopulations, the immune landscape of ESCC was established. The workflow of scRNA-seq analysis is shown in Figure 1A. First, the major cell subpopulations were clustered and annotated, and each major cell population was re-clustered (Figure 1A). The signature marker genes for each cell subset were identified using the Seurat toolkit (16). Next, the RNA-seq dataset for ESCC was acquired from TCGA database (Figure 1B), and the GSVA score of the

gene signature specific to each cellular subset was calculated for each ESCC RNA-seq data set based on the gene signatures of each cellular subset (Figure 1C) to estimate the correlation between GSVA score and survival probability (Figure 1D).

The scRNA-seq cluster numbers were assigned from the largest cell population (Cluster 0) to the smallest (Cluster 9) (Figure 1E). The characteristic gene markers in each cluster are shown in Figure 1F. The cell distribution Frequency is shown in Figure 1G.

The largest single-cell constituent Cluster 0 cells were T lymphocytes with specific gene expression including *BATF*, *IL32* and *CTLA4* (Figure 1F) (17-19). Cluster 1 cells were MΦ, expressing *SPP1*, *CXCL2* and *CTSB* (Figure 1F) (20-22). Cluster 2 represented B lymphocytes with high expression of *IGHG1*, *IGHG2* and *IGKC* (Figure 1F) (23,24). Cluster 3 represented NK cells that expressed *GNLY*, *NKG7* and *KLRD1* (Figure 1F) (25-27). Cluster 4 was tissue stem cells with special genes including *HST1H4C*, *STMN1* and *TUBA1B* (Figure 1F) (28,29). Cluster 5 cells were granulocytes with special genes including *PI3*, *CXCL8* and *SLPI* (Figure 1F) (30-32). Cluster 6 cells were DC cells expressing *HLA-DRA*, *HLA-DPA1*, and *CCL17* (Figure 1F) (33-35). Cluster 7 represented mast cells expressing *TPSAB1*, *TPSAB2* and *CPA3* (Figure 1F) (36-38). Cluster 8 cells appeared to be a pDC (plasmacytoid dendritic cell) cell subset expressing *IRF4*, *TCL1A* and *AREG* (Figure 1F) (39,40). Cluster 9 cells represented endothelial cell expressing *COL1A1*, *COL6A2* and *S100A2* (Figure 1F) (41-43). In addition, the distribution frequency of each major cluster is showed in Figure 1G among the different patients and no cellular cluster was derived from a single patient. Overall, the major cellular clusters forming the ESCC TME were profiled.

Exhausted CD4⁺ T (ExbCD4T) cells correlated with poor prognosis and liver metastasis

T cells regulate the ESCC TME by secreting specific cytokines and interacting with other immune cells (44,45), so they were further re-clustered to investigate the effect of the T cell subsets in the prognosis and liver metastasis of ESCC patients.

There were 6 T-cell subsets from Cluster 0 to Cluster 5 (Figure 2A,2B). UMAP of scRNA-seq data visualizing the special gene markers is showed in Figure 2C). Cluster 0 cells were cytotoxic T (CytT) cells expressing *CCL5*, *NKG7* and

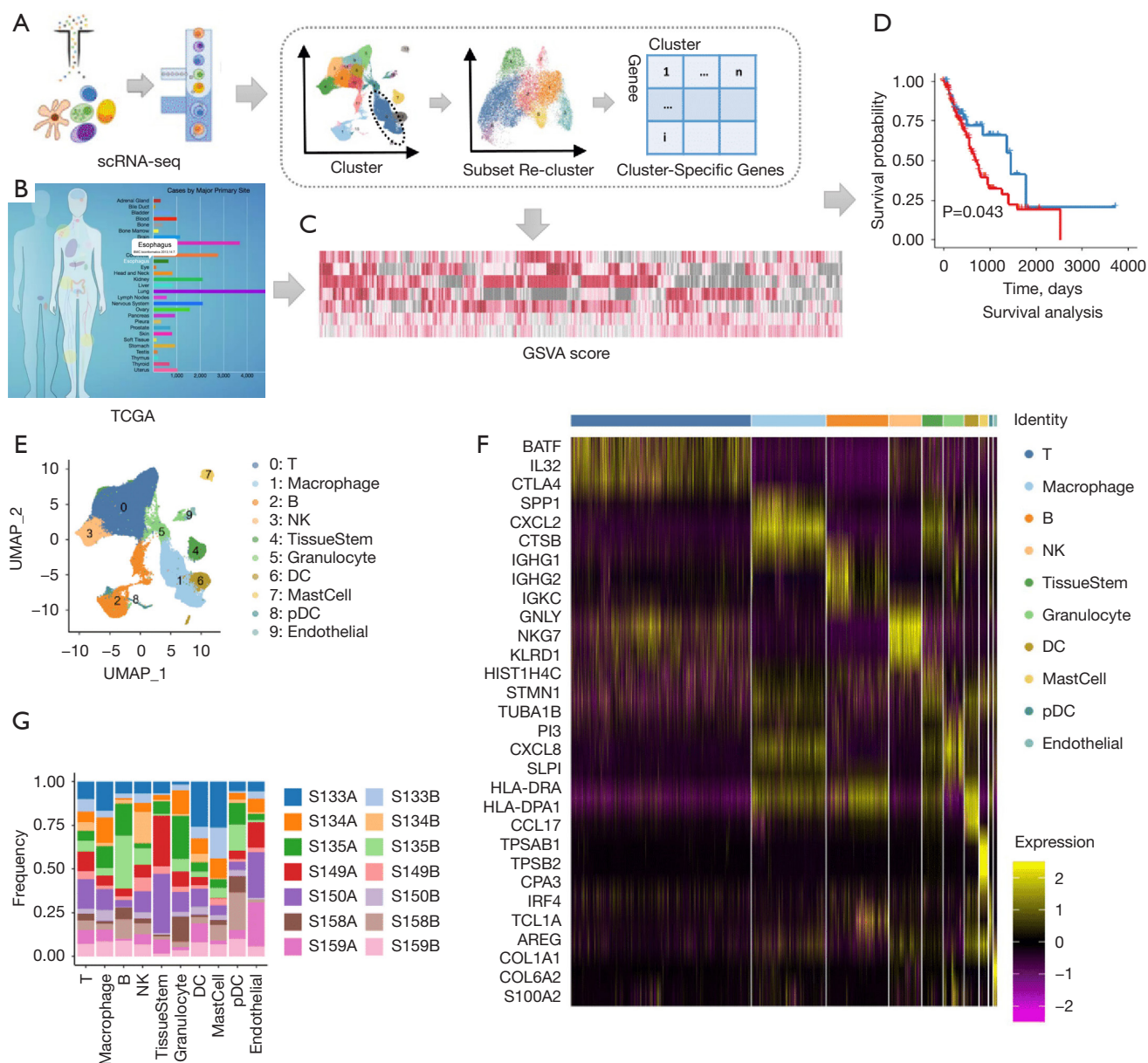


Figure 1 scRNA-seq clustering analysis for ESCC. (A) Overview of the workflow; (B) TCGA dataset analysis; (C) heatmap of the distribution of the assigned gene sets by GSVAscores; (D) survival curves for Low/High GSVAscore groups; (E) UMAP of scRNA-seq data visualizing 10 cell clusters marked 0–9; (F) heatmap of differentially expressed genes in each cluster, yellow to dark purple: high to low expression; (G) distribution frequency of cluster cells. scRNA-seq, single-cell RNA sequencing; TCGA, The Cancer Genome Atlas; GSVAscore, gene set variation analysis; UMAP, Uniform Manifold Approximation and Projection; NK, natural killer; DC, dendritic cell; pDC, plasmacytoid dendritic cell; ESCC, esophageal squamous cell carcinoma.

GZMB (46,47) (Figure 2B), and *CD8A* (Figure 2 C3) (48). Cluster 1 cells represented regulatory T cells (Tregs) with *TNFRSF4*, *BATF* and *FOXP3* expression (Figure 2B, Figure 2 C4) (49–51), and *CD4* (Figure 2 C2) (52). Cluster 2 cells

were resident CD4 T (ResCD4⁺ T) cells with *IL7R*, *KLRB1* and *FOS* expression (Figure 2B) (53–55). Cluster 3 cells were naïve CD4⁺ T cells expressing *SELL*, *PASK* and *LEF1* (Figure 2B) (56), and *CCR7* (Figure 2 C6) (57). Cluster 4

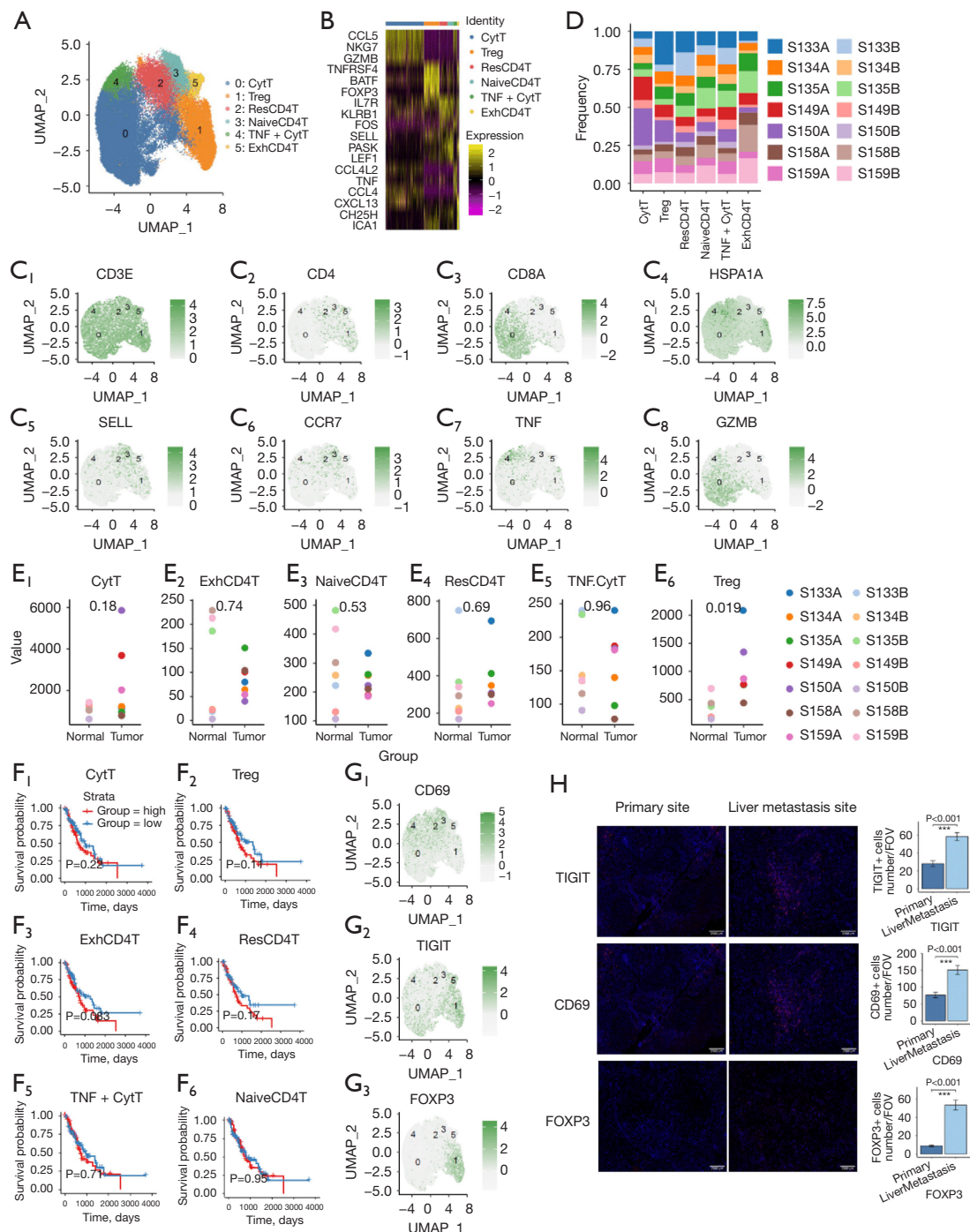


Figure 2 Analysis of cell subset of T cells. (A) UMAP of scRNA-seq data visualizing 6 cell clusters marked 0–5; (B) heatmap of differentially expressed genes in each cluster, Yellow to dark purple: high to low expression; (C) UMAP of scRNA-seq data visualizing the special gene markers; (D) distribution frequency of cluster cells; (E) expression values of cluster cells in normal and tumor groups; (F) survival curves for low/high expression group; (G) feature plot of CD69 (resident T cell marker), TIGIT (exhausted T cell marker), and FoxP3 (regulatory T cell marker), shown in UMAP; (H) multiplex immunohistochemistry assays for TIGIT, CD69 and FoxP3. Scale bar =250 μ m. ***, $P<0.001$. UMAP, Uniform Manifold Approximation and Projection; CytT, cytotoxic T; Treg, regulatory T cell; NaiveCD4T, naive CD4⁺ T cell; TNF, tumor necrosis factor; ExhCD4T, exhausted CD4⁺ T cell; ResCD4T, resident CD4⁺ T cell; FOV, field of view; scRNA-seq, single-cell RNA sequencing.

cells were TNF⁺ CytT cells with specific genes including *CCL4L2*, *TNF* and *CCL4* (Figure 2B, Figure 2 C7) (58,59). Cluster 5 cells were ExhCD4⁺ T cells expressing *CXCL13*, *CH25H* and *ICA1* (Figure 2B) (60,61). We found that the frequency of Cluster 0 (CytT) and Cluster 1 (Tregs) was higher in the tumor group than in the normal group (Figure 2D,2E).

Next, we calculated the T-cell subset specific score based on the feature genes belonging to each subset. We found the CytT-specific and Treg-specific GSVA scores did not correlate with patients' prognosis. Only the Cluster 5 (ExhCD4⁺ T) cell subset was negatively related to the ESCC patients' prognosis (Figure 2F). Furthermore, mIHC staining was used to confirm some of the marker genes representing the key cellular subsets. *CD69*, *TIGIT* and *FoxP3* were not only detected in the specific subsets based on scRNA-seq data (Figure 2G), these genes were signature markers as well. *CD69* is the key marker for resident T cells (62). *TIGIT* could be used to identify exhausted T cells (63) and *FoxP3* is the master transcription factor for Tregs (64).

We found there were more TIGIT⁺ ExhCD4⁺ T cells, CD69⁺ ResCD4⁺ T cells and FoxP3⁺ Tregs in the ESCC liver metastasis site than in the primary site and the quantification was also added for key cell signatures (Figure 2H). Thus, we identified key T-cell subsets associated with the prognosis and liver metastasis of ESCC patients.

Increased TolPlaB cells in liver metastasis associated with poor prognosis of ESCC patients

B lymphocytes are primarily responsible for basic functions such as antibody production (65). However, the phenotypic and functional diversity of B lymphocytes also results in independent regulatory roles in the immune response (65). To explore the role of B-cell subpopulations in ESCC patients' prognosis and liver metastasis, B cells were re-clustered. Firstly, the B cells were divided into 4 cell subsets (Figure 3A,3B). UMAP of scRNA-seq data visualizing the special gene markers is showed in Figure 3C Cluster 0 cells were active B (ActB) cells expressing *CD69*, *CD83* and *HLA-DRA* (Figure 3B, Figure 3 C3) (66,67). Cluster 1 cells were plasma B (PlaB) cells with *IGHG1*, *IGHG2* and *IGKV3-20* expression (Figure 3B, Figure 3 C1, C2). Cluster 2 cells were proliferating B (ProlB) cells expressing *TUBA1B*, *H2AFZ*, *HIST1H4C* and *MKI67* (Figure 3B, Figure 3 C5). Cluster 3 cells were TCL1A⁺ tolerance plasma B (TolPlaB) cells expressing *TCL1A*, *LRMP* and *PRPSAP2*

(Figure 3B, Figure 3 C4) (68,69). The results showed that the number of Cluster 1 (PlaB) and Cluster 3 (TolPlaB) cells were upregulated in the tumor group compared with the normal group (Figure 3D,3E), although only the TCL1A⁺ TolPlaB-specific GSVA score was associated with poor prognosis (Figure 3F). We found TCL1A⁺ TolPlaB cells were also increased in the liver metastasis site compared with the ESCC primary site (Figure 3G). Thus, increased numbers of TolPlaB cells (Cluster 3) in the ESCC liver metastasis site was associated with poor prognosis.

Contribution of CMTM2⁺ neutrophil cell subset in ESCC liver metastasis site to shorter survival time in ESCC patients

Granulocytes participate in a series of tightly controlled molecular processes to regulate tumor immunity (70). To analyze the effect of granulocyte cell subsets in ESCC and its clinical significance, the cell populations were re-clustered and analyzed. The granulocyte cells included 3 cellular subsets (Figure 4A,4B). UMAP of scRNA-seq data visualizing the special gene markers is showed in Figure 4C. Cluster 0 cells were monocyte cells with *CCL3L1*, *PI3* and *CCL3* expression (71,72) (Figure 4B). Cluster 1 cells represent S100A10⁺ neutrophil cells with *S100A9*, *S100A2* and *SFN* expression (Figure 4B, Figure 4 C3, C4) (73,74). Cluster 2 cells were CMTM2⁺ neutrophil cells with *CMTM2*, *S100A9* and *S100A12* expression (Figure 4B, Figure 4 C1, C2, C5).

Please note that myeloid cells, including monocytes and neutrophils, in the tumor site are also referred to as myeloid-derived suppressor cells (MDSCs) (75). Therefore, MDSCs can be categorized as monocytic MDSCs (M-MDSC) and polymorphonuclear MDSCs (PMN-MDSCs) (75). Neutrophils and PMN-MDSCs share the same origin and many morphological and phenotypic features (75). Thus S100A9⁺ neutrophil cells defined here may also represent the so-called MDSCs, which could perform their immune-suppressive activity through S100A8 and S100A9 (76).

The counts of Cluster 0 (monocyte) and Cluster 1 (S100A10⁺ neutrophils) were elevated in the tumor group compared with the normal group (Figure 4D,4E), but only the CMTM2⁺ neutrophil-specific GSVA score was associated with patients' poor prognosis. The monocytes and S100A10⁺ neutrophil-specific GSVA scores were not correlated with patients' prognosis (Figure 4F). Furthermore, we found there were more CMTM2⁺

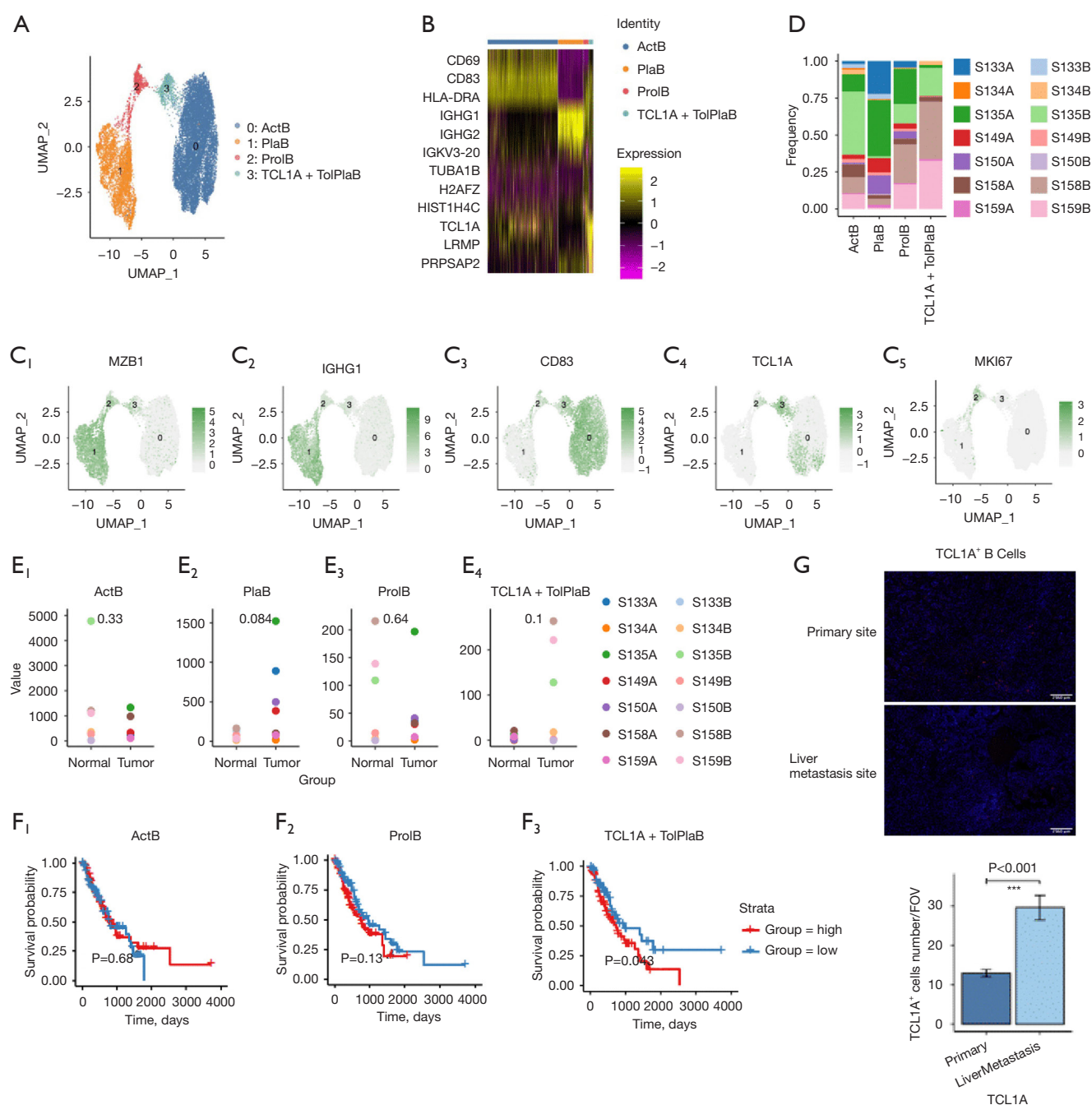


Figure 3 Analysis of cell subset of B cells. (A) UMAP of scRNA-seq data visualizing 4 cell clusters marked 0–3; (B) heatmap of differentially expressed genes in each cluster. Yellow to dark purple: high to low expression; (C) UMAP of scRNA-seq data visualizing the special gene markers; (D) distribution frequency of cluster cells; (E) expression values of cluster cells in normal and tumor group; (F) survival curves for low/high expression groups; (G) multiplex immunofluorescence assay for TCL1A⁺ B cells. Scale bar =250 μm. ***, P<0.001. UMAP, Uniform Manifold Approximation and Projection; ActB, active B; PlaB, plasma B; ProlB, proliferating B; TolPlaB, tolerance plasma B; FOV, field of view; scRNA-seq, single-cell RNA sequencing.

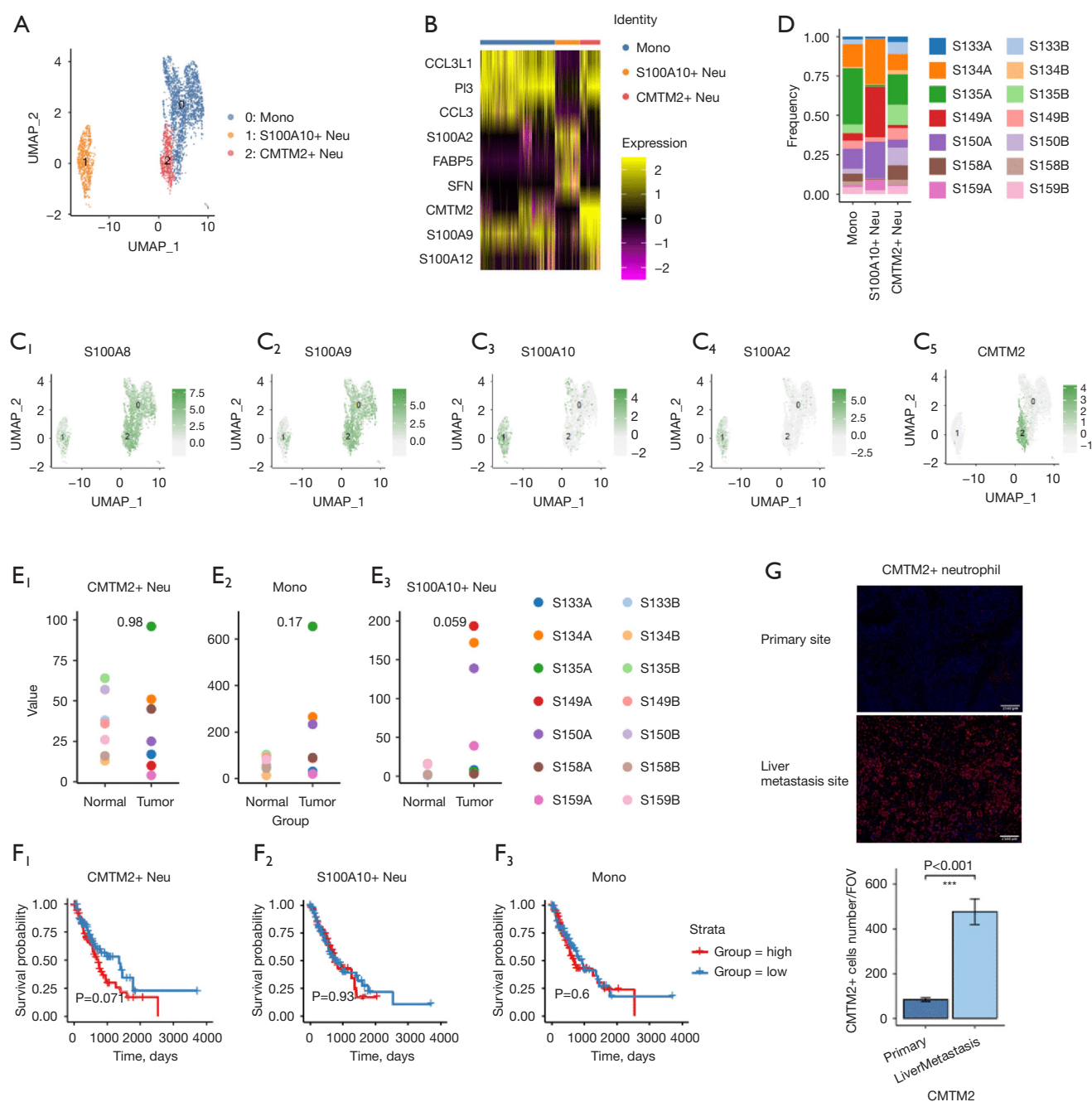


Figure 4 Analysis of cell subset of granulocytes. (A) UMAP of scRNA-seq data visualizing 3 cell clusters marked 0–2; (B) heatmap of differentially expressed genes in each cluster. Yellow to dark purple: high to low expression; (C) UMAP of scRNA-seq data visualizing the special gene markers; (D) distribution frequency of cluster cells; (E) expression values of cluster cells in normal and tumor groups; (F) survival curves for low/high expression groups; (G) multiplex immunohistochemistry assay for CMTM2⁺ neutrophils. Scale bar =250 μ m. ***, $P<0.001$. UMAP, Uniform Manifold Approximation and Projection; Mono, monocyte; Neu, neutrophil; FOV, field of view; scRNA-seq, single-cell RNA sequencing.

neutrophil cells in the liver metastasis site than in the ESCC primary site (Figure 4G). Therefore, the increased CMTM2⁺ neutrophil cell proportion in the liver metastasis may contribute to shorter survival time and worse prognosis.

Effect of elevated natural killer T (NKT) cell subset in the primary site on prognosis in ESCC patients

NK cells, as cytotoxic lymphocytes of the innate immune system, can effectively kill cancerous cells. However, they are highly heterogeneous in the TME (77). Hence, the cell subset of NK cells was re-clustered to explore the role of the diverse NK cell subpopulation in ESCC.

The NK cells were re-clustered to 5 subsets (Figure 5A,5B). UMAP of scRNA-seq data visualizing the special gene markers is showed in Figure 5C. Cluster 0 cells were NK cells expressing *KH2D1B*, *HIR2DL3* and *INC02446* expression (Figure 5B) (78,79). Cluster 1 cells were ILC3b cells with *KRT81* expression (Figure 5B) (80). Cluster 2 cells were NKT cells with *PRSS23*, *FGFBP2* and *GZMH* expression (Figure 5B) (81). Cluster 3 cells were spondin 2 (SPON2)⁺ NK cells with *SPON2* expression (Figure 5B) (81). Cluster 4 cells were $\gamma\delta$ NKT cells expressing *TRDV2*, *TRGV9* and *CD3E* (Figure 5B, Figure 5C4) (82,83). In addition, the distribution frequency of each NK cell subsets was shown in Figure 5D among the different patients and no subset was derived from a single patient. However, we did notice NKT and SPON2⁺ NK subsets were quite obvious in patient S134 para-tumoral site (Figure 5D).

Cluster 2 (NKT), Cluster 3 (SPON⁺ NK) and Cluster 4 ($\gamma\delta$ NKT) cells were higher in the tumor group than in the normal group (Figure 5E), but it seemed that only Cluster 2 (NKT) cells were associated with better prognosis of ESCC patients (Figure 5F).

In the liver metastasis site, there were also fewer Cluster 2 (NKT) cells than in the primary ESCC site (Figure 5G), which suggested that an increased NKT cell subset in the primary site may induce a better prognosis in ESCC patients.

Effect of elevated C1QA/B⁺ MΦ subset in liver metastasis site on prognosis in ESCC patients

As an essential innate immune population, TAMs perform diverse functions to maintain homeostasis and ward off foreign pathogens. They are also pivotal for driving tumor

progression, metastasis, and resistance to therapy (84). To elucidate the special function of different subsets, the MΦ subset was re-clustered. The results showed there were 8 cell subsets from Cluster 0 to Cluster 7 (Figure 6A,6B). UMAP of scRNA-seq data visualizing the special gene markers is showed in Figure 6C. Cluster 0 cells were infiltrating MΦ (InfMΦ) with *IL1B*, *CCL20* and *G0S2* expression (Figure 6B) (85,86). Cluster 1 cells were C1QA/B⁺ resident MΦ (C1QA/B⁺ ResMΦ) cells with *C1QA*, *C1QB* and *APOE* expression (Figure 6B, Figure 6 C1, C2) (87,88). Cluster 2 cells were CD206⁺ MΦ cells with *CD206* and *GPR183* expression (Figure 6B) (89). Cluster 3 cells were CTSK⁺ resident MΦ (CTSK⁺ ResMΦ) cells with *CTSK*, *APOC1* and *CCL18* expression (Figure 6B, Figure 6 C3) (90,91). Cluster 4 cells were IDO1⁺ MΦ cells with *IDO1*, *CXCL10*, *ISG15* and *APOBEC3A* expression (Figure 6B) (92,93). Cluster 5 cells were SPP1⁺ MΦ cells with *SPP1*, *CXCL10*, *ISG15* and *APOBEC3A* expression (Figure 6B, Figure 6 C4). Cluster 6 cells were Mono cells with *CXCL8* and *PI3* expression (Figure 6B) (94,95). Cluster 7 cells were proliferating MΦ (ProMΦ) with *TUBA1B*, *STMN1* and *HIST1H4C* expression (Figure 6B, Figure 6 C5).

The Cluster 0 (C1QA/B ResMΦ), Cluster 1 (CD206⁺ MΦ), Cluster 2 (CTSK⁺ MΦ) and Cluster 7 (Spp1⁺ MΦ) cells were higher in the tumor group than in the normal group (Figure 6D, Figure 6E). The GSVA score was calculated using bulk RNA-Seq data obtained from TCGA based on MΦ subset feature genes. The correlation between the subset-specific GSVA score and patients' prognosis was investigated. We found survival time was shorter in the High group than in the Low group based on the GSVA score of the C1QA/B⁺ MΦ subset (Figure 6F). We also observed more C1QA/B MΦ in the liver metastasis site than in the primary ESCC site (Figure 6G). The results revealed that an elevated C1QA/B⁺ MΦ subset was associated with liver metastasis and poor prognosis in ESCC patients.

Role of C1QA/B⁺ TAMs in ESCC

To identify the key cell subset regulating the ESCC TME, cell-cell interactions were analyzed. The results showed that the C1QA/B⁺ MΦ subset was closely associated with other cell subsets (Figure 7A), and the absolute value of the correlation coefficient was maximum for C1QA/B⁺ MΦ (Figure 7B).

To visualize the interrelationships among the different cell subsets, we first calculated the correlation coefficient between any two subsets within TCL1A⁺ TolPlaB cells,

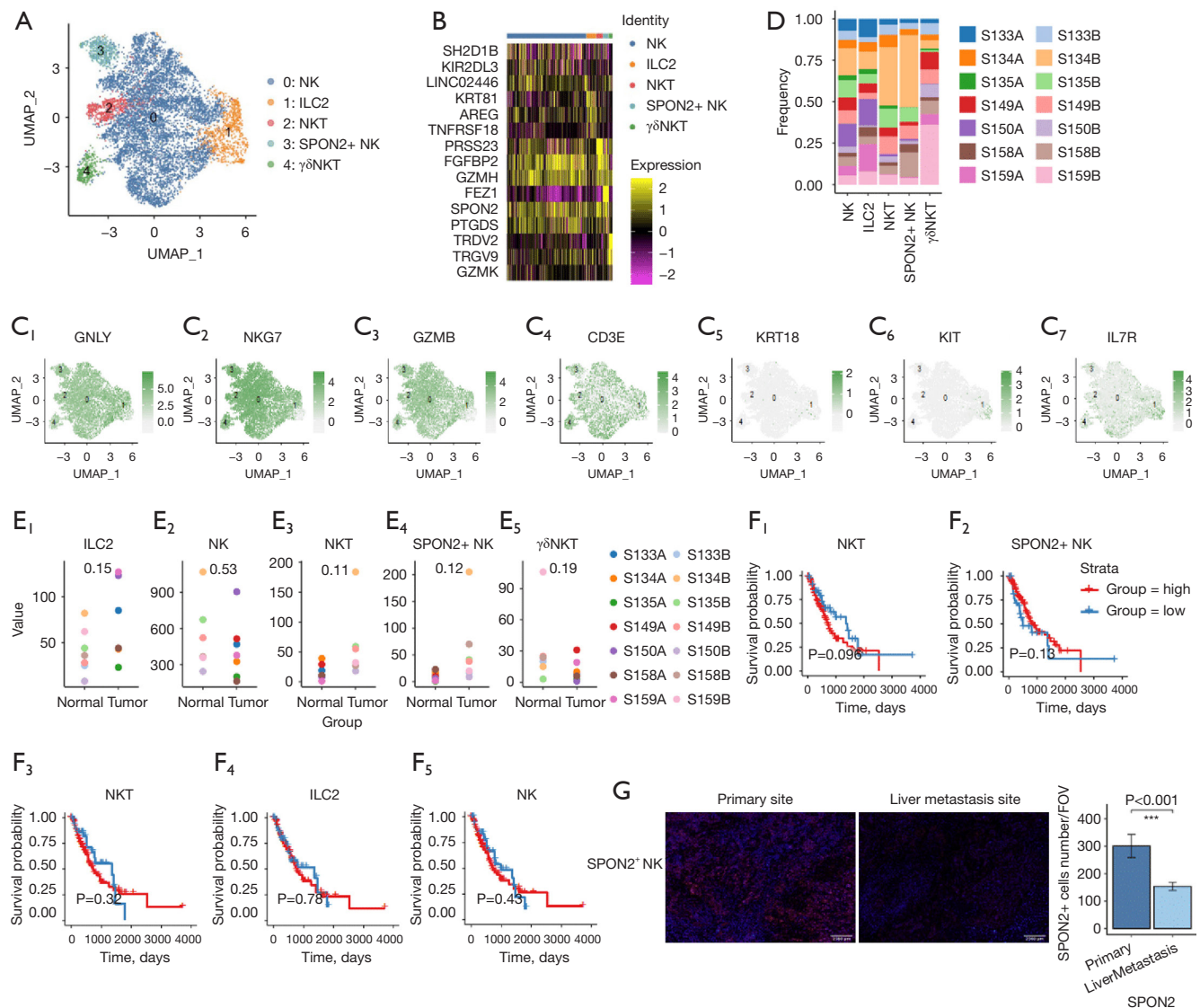


Figure 5 Analysis of NK cell subset. (A) UMAP of scRNA-seq data visualizing 5 cell clusters marked 0–4; (B) heatmap of differentially expressed genes in each cluster. Yellow to dark purple: high to low expression; (C) UMAP of scRNA-seq data visualizing the special gene markers; (D) distribution frequency of cluster cells; (E) expression values of cluster cells in normal and tumor groups; (F) survival curves for low/high expression groups; (G) multiplex immunohistochemistry assay for SPON2⁺ NK cells. Scale bar =250 μ m. ***, $P<0.001$. UMAP, Uniform Manifold Approximation and Projection; ILC2, type 2 innate lymphoid cells; NK, natural killer; NKT, natural killer T; SPON2, spondin 2; FOV, field of view; scRNA-seq, single-cell RNA sequencing.

CMTM2⁺ neutrophils, C1QA⁺/B⁺ MΦ, NKT cells, SPON2⁺ NK cells, Tregs, ResCD4⁺ T cells and ExhCD4⁺ T cells. A circular chord diagram was constructed to visualize the correlation ecoefficiency weight between the different cell subsets, and the results showed that C1QA/B⁺ MΦ had more connections with other cell subsets (Figure 7C). Other than C1QA/B⁺ MΦ, CMTM2⁺ neutrophils also had

multiple connections, indicating that CMTM2⁺ neutrophils could also mediate important immune-suppressive roles in the ESCC TME, associated with worse prognosis.

We wanted to investigate the interaction between C1QA/B⁺ MΦ and other cell subpopulations. Firstly, the expression of myeloid immune checkpoints was portrayed in C1QA/B⁺ MΦ. The results showed that CD274, PDCD1LG2,

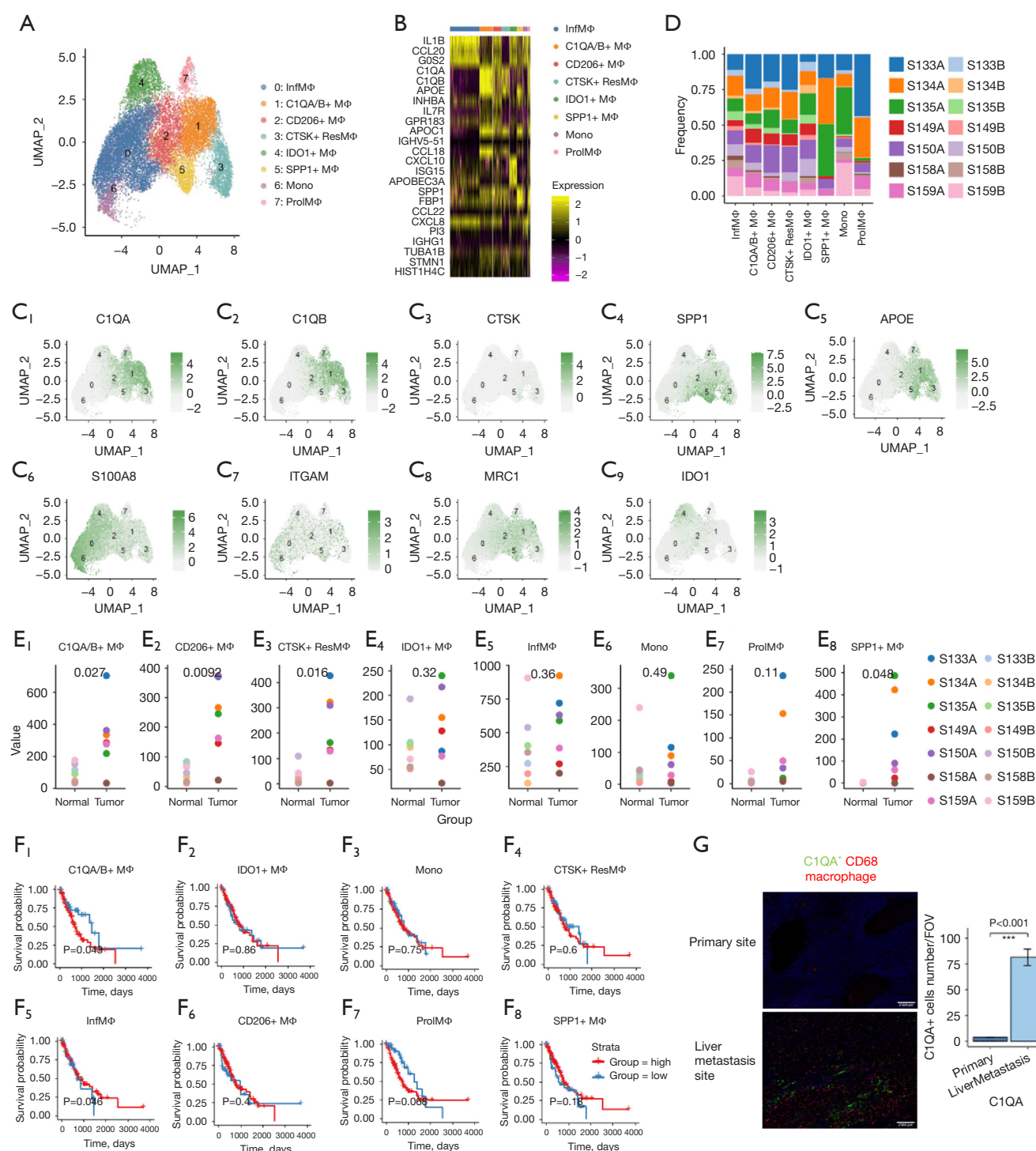


Figure 6 Analysis for cell subset of macrophages. (A) UMAP of scRNA-seq data visualizing 8 cell clusters marked 0–7; (B) heatmap of differentially expressed genes in each cluster. Yellow to dark purple: high to low expression; (C) UMAP of scRNA-seq data visualizing the special gene markers; (D) distribution frequency of cluster cells; (E) expression value of cluster cells in normal and tumor groups; (F) survival curves for low/high expression groups; (G) multiplex immunohistochemistry assay for C1QA⁺ CD68⁺ macrophages. Scale bar = 250 μm. ***, $P < 0.001$. UMAP, Uniform Manifold Approximation and Projection; InfMΦ, infiltrating macrophages; MΦ, macrophage; Mono, monocyte; ResMΦ, resident macrophage; ProlMΦ, proliferating macrophage; FOV, field of view; scRNA-seq, single-cell RNA sequencing.

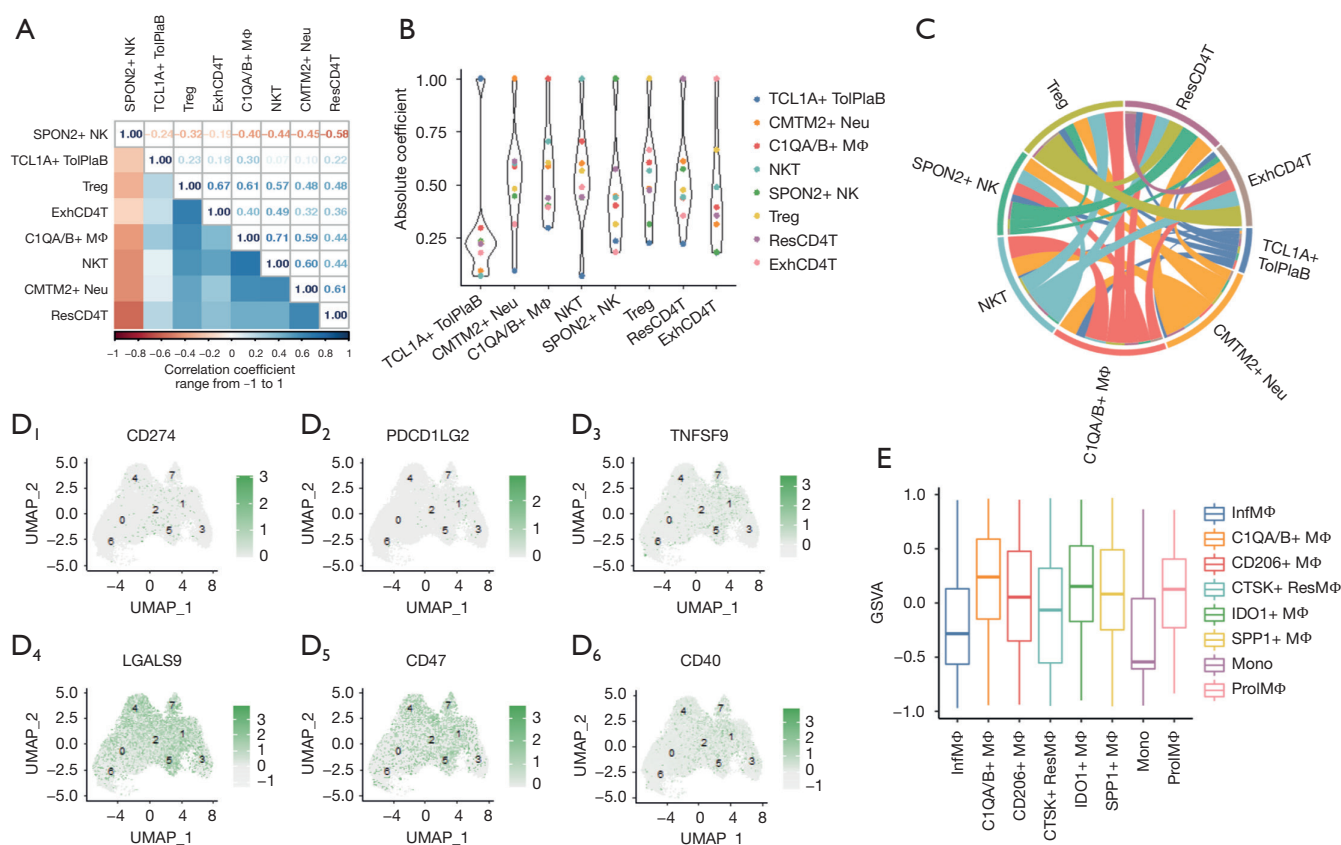


Figure 7 Role of C1QA/B⁺ tumor-associated macrophages in esophageal squamous cell carcinoma. (A) Principal component analysis; (B) absolute value of correlation coefficient; (C) circular chord diagram to describe the correlation; (D) UMAP of scRNA-seq data visualizing the special gene markers; (E) GSVA scores for different cell subsets. UMAP, Uniform Manifold Approximation and Projection; SPON2, spondin 2; NK, natural killer; NKT, natural killer T; Treg, regulatory T cell; ExhCD4T, exhausted CD4⁺ T; Neu, neutrophil; ResCD4T, resident CD4⁺ T; Mono, monocyte; GSVA, gene set variation analysis; scRNA-seq, single-cell RNA sequencing; InfMΦ, infiltrating macrophage; MΦ, macrophage; ResMΦ, resident macrophage; ProlMΦ, proliferating macrophage.

TNFSF9, *CD40*, *LGALS9* and *CD47* positively correlated to Cluster 8 (C1QA/B⁺ MΦ) (Figure 7D). Next, the gene signature was established based on these myeloid immune checkpoints, and the GSVA score was calculated. The score is the highest in the C1QA/B⁺ MΦ cell subset (Figure 7E), which indicated that C1QA/B⁺ MΦ may play a central role by expressing myeloid immune checkpoints to mediate the immune microenvironment of ESCC, and thereby influence patients' prognosis.

Discussion

The TME is complex and continuously evolving, which plays a crucial role in tumor homeostasis (96). In this study, multi-omics profiling of the ESCC TME was

performed using scRNA-seq and RNA-Seq data. The gene signatures were established, and the specific GSVA scores were calculated. Thereafter, the GSVA score was utilized to investigate the correlation between cell subset abundance and survival probability, and the crucial cell subsets were screened and identified. Generally, single-cell transcriptome analyses were conducted to assess the cellular heterogeneity in normal and tumor tissues. In this study, 10 cell populations were identified such as T lymphocytes, B lymphocytes, granulocytes, NK cells, and MΦ. Major cell populations were re-clustered, the specific gene signature was described and the survivorship curve was drawn to investigate the role of the cell subset in ESCC.

Tregs play a critical role in the maintenance of self-tolerance and suppressing aberrant immune responses.

Treg infiltration promotes tumor growth and invasion in ESCC (97). Accumulating evidence suggests that the removal of Tregs could evoke and enhance an anti-tumor immune response (98). Our results also indicated that the higher the proportion of Tregs, the shorter survival time of the patient. The percentage of CD4⁺ T cells is an indicator of cellular immunity and they have a unique role in promoting tumor eradication, which implies CD4⁺ T cells could influence the prognosis of ESCC (99). However, our results showed that upregulation of the ResCD4⁺ T and ExhCD4⁺ T cell subpopulations resulted in worse prognosis in ESCC patients, which may identify the unique function of specific CD4 T-cell subsets.

Tumor-infiltrating B lymphocytes play a pivotal role in shaping tumor development and promoting/suppressing tumor growth (100). Previous study indicated that enhanced *TCL1A*, an oncogene, results in an aggressive cellular and clinical phenotype (101). *TCL1A* is positively associated with various hematological malignancies by its effect on the infiltration of B cells and dendritic cells (102,103). *TCL1A* also plays an important role in promoting multi-modal tumor resistance (104). In this study, we also found the ESCC patients' prognosis was worse when the proportion of TCL1A⁺ TolPlaB cells was significantly upregulated.

Granulocytes, as the most abundant leukocytes in human blood, are involved in the immune response against cancer (70). Previous study showed that *CMTM2* down-regulation induces hepatocellular carcinoma metastasis by promoting the epithelial-mesenchymal transition process (105). In our study, the survival time was shorter when the CMTM2⁺ neutrophil cell proportion increased, which was in accord with previous reports conducted to predict the progression of ESCC.

TAMs promote tumor growth and metastasis by enhancing cancer cell proliferation, immunosuppression, and angiogenesis (106). In the ESCC TME, MΦ infiltration could promote tumor vascularity and chemoresistance via monocyte chemoattractant protein - 1 (MCP-1) and IL34, respectively (107,108). Macrophages could also contribute to ESCC tumor progression through the AKT and ERK signaling pathways via GDF15 (109) and the CCL3-CCR5 axis (110). In addition, MΦ could also promote proliferation and invasion of ESCC via EGF (epidermal growth factor) production (111).

C1QA plays a significant role in the innate immune response by counteracting the C1Q receptor (112). Additionally, related research has revealed that C1QA and C1QB are potential indicators of the tumorigenesis and

development of osteosarcoma (113). Interestingly, our results suggested that C1QA/B⁺ TAMs were the central regulator of the ESCC TME, closely associated with several key cell subsets. In terms of mechanism, several immune checkpoints, including CD40, CD47 and LGALS9, showed positive expression in C1QA/B⁺ MΦ. The CD47 protein plays a pivotal role in tumors by delivering a “don't eat me signal”, and targeting CD47 regulates the cancer cell fate (114). Therefore, we speculate that C1QA/B⁺ TAMs may exert a central regulatory effect in immune evasion of ESCC via multiple immune checkpoint expressions. In addition, a previous report showed that tumor cells could hijack MΦ-produced complement C1Q molecules to promote tumor growth (115), and such a mechanism might also exist in the ESCC TME. Current immunotherapy mainly depends on the PD-1/PD-L1 axis, which targets T cell exhaustion. Immunotherapy relies on MΦ targets is still lacking. Here, we identified the C1QA⁺ MΦ as the central interacting immune cells during immunosuppression loop formation. C1QA⁺ MΦ carries many immune checkpoints, and future immunotherapy could target C1QA⁺ MΦ as an alternative option when T cells are spared in the tumor immune microenvironment.

We mainly applied scRNA-seq, mIHC and transcriptomic to study ESCC. Epigenetic landscape is very important for the ESCC study; however, our current tools setting is not able to capture the epigenetic landscape. In addition, C1QA⁺ MΦ subset distribution and contribution at various ESCC stages were not revealed since only few pairs of tissues were included for scRNA-seq analysis.

Conclusions

Our results indicated that C1QA/B⁺ MΦ maybe a potential immunotherapy target for ESCC. Deletion of this cell subset may increase the efficacy of immunotherapy by mediating myeloid immune checkpoint expressions, and thereby influence the ESCC patients' prognosis.

Acknowledgments

Funding: This work was supported by the National Natural Science Foundation of China (No. 82173051); the Joint Funds for the Innovation of Science and Technology, Fujian province (No. 2019Y9036); Scientific Research Foundation of Fujian Cancer Hospital (No. 2021YN01); Fujian Provincial Clinical Research Center for Cancer Radiotherapy and Immunotherapy (No. 2020Y2012);

National Clinical Key Specialty Construction Program (No. 2021); Fujian Clinical Research Center for Radiation and Therapy of Digestive; Respiratory and Genitourinary Malignancies and the National Clinical Key Specialty Construction Program.

Footnote

Reporting Checklist: The authors have completed the MDAR reporting checklist. Available at <https://atm.amegroups.com/article/view/10.21037/atm-22-5351/rc>

Data Sharing Statement: Available at <https://atm.amegroups.com/article/view/10.21037/atm-22-5351/dss>

Conflicts of Interest: All authors have completed the ICMJE uniform disclosure form (available at <https://atm.amegroups.com/article/view/10.21037/atm-22-5351/coif>). The authors have no conflicts of interest to declare.

Ethical Statement: The authors are accountable for all aspects of the work in ensuring that questions related to the accuracy or integrity of any part of the work are appropriately investigated and resolved. The study was conducted in accordance with the Declaration of Helsinki (as revised in 2013). The study was approved by the ethics committee of Fujian Cancer Hospital (No. 10104700) and informed consent was taken from all individual participants.

Open Access Statement: This is an Open Access article distributed in accordance with the Creative Commons Attribution-NonCommercial-NoDerivs 4.0 International License (CC BY-NC-ND 4.0), which permits the non-commercial replication and distribution of the article with the strict proviso that no changes or edits are made and the original work is properly cited (including links to both the formal publication through the relevant DOI and the license). See: <https://creativecommons.org/licenses/by-nc-nd/4.0/>.

References

1. Arnold M, Soerjomataram I, Ferlay J, et al. Global incidence of oesophageal cancer by histological subtype in 2012. *Gut* 2015;64:381-7.
2. Abnet CC, Arnold M, Wei WQ. Epidemiology of Esophageal Squamous Cell Carcinoma. *Gastroenterology* 2018;154:360-73.
3. Engel LS, Chow WH, Vaughan TL, et al. Population attributable risks of esophageal and gastric cancers. *J Natl Cancer Inst* 2003;95:1404-13.
4. Shimada H, Nabeya Y, Okazumi S, et al. Prediction of survival with squamous cell carcinoma antigen in patients with resectable esophageal squamous cell carcinoma. *Surgery* 2003;133:486-94.
5. Torre LA, Siegel RL, Ward EM, et al. Global Cancer Incidence and Mortality Rates and Trends--An Update. *Cancer Epidemiol Biomarkers Prev* 2016;25:16-27.
6. Zheng Y, Chen Z, Han Y, et al. Immune suppressive landscape in the human esophageal squamous cell carcinoma microenvironment. *Nat Commun* 2020;11:6268.
7. Kuo HY, Guo JC, Hsu CH. Anti-PD-1 immunotherapy in advanced esophageal squamous cell carcinoma: A long-awaited breakthrough finally arrives. *J Formos Med Assoc* 2020;119:565-8.
8. Darmanis S, Sloan SA, Croote D, et al. Single-Cell RNA-Seq Analysis of Infiltrating Neoplastic Cells at the Migrating Front of Human Glioblastoma. *Cell Rep* 2017;21:1399-410.
9. Baba Y, Nomoto D, Okadome K, et al. Tumor immune microenvironment and immune checkpoint inhibitors in esophageal squamous cell carcinoma. *Cancer Sci* 2020;111:3132-41.
10. Lavin Y, Kobayashi S, Leader A, et al. Innate Immune Landscape in Early Lung Adenocarcinoma by Paired Single-Cell Analyses. *Cell* 2017;169:750-765.e17.
11. Zhang Q, He Y, Luo N, et al. Landscape and Dynamics of Single Immune Cells in Hepatocellular Carcinoma. *Cell* 2019;179:829-845.e20.
12. Savas P, Virassamy B, Ye C, et al. Single-cell profiling of breast cancer T cells reveals a tissue-resident memory subset associated with improved prognosis. *Nat Med* 2018;24:986-93.
13. Stuart T, Butler A, Hoffman P, et al. Comprehensive Integration of Single-Cell Data. *Cell* 2019;177:1888-1902.e21.
14. Hänzelmann S, Castelo R, Guinney J. GSEA: gene set variation analysis for microarray and RNA-seq data. *BMC Bioinformatics* 2013;14:7.
15. Obradovic A, Chowdhury N, Haake SM, et al. Single-cell protein activity analysis identifies recurrence-associated renal tumor macrophages. *Cell* 2021;184:2988-3005.e16.
16. Macosko EZ, Basu A, Satija R, et al. Highly Parallel Genome-wide Expression Profiling of Individual Cells Using Nanoliter Droplets. *Cell* 2015;161:1202-14.
17. Punkenburg E, Vogler T, Büttner M, et al. Batf-dependent

- Th17 cells critically regulate IL-23 driven colitis-associated colon cancer. *Gut* 2016;65:1139-50.
18. Dinarello CA, Kim SH. IL-32, a novel cytokine with a possible role in disease. *Ann Rheum Dis* 2006;65 Suppl 3:iii61-4.
 19. Jiang P, Gu S, Pan D, et al. Signatures of T cell dysfunction and exclusion predict cancer immunotherapy response. *Nat Med* 2018;24:1550-8.
 20. Morse C, Tabib T, Sembrat J, et al. Proliferating SPP1/MERTK-expressing macrophages in idiopathic pulmonary fibrosis. *Eur Respir J* 2019;54:1802441.
 21. De Filippo K, Dudeck A, Hasenberg M, et al. Mast cell and macrophage chemokines CXCL1/CXCL2 control the early stage of neutrophil recruitment during tissue inflammation. *Blood* 2013;121:4930-7.
 22. Sandler M, Weiss FU, Golchert J, et al. Cathepsin B-Mediated Activation of Trypsinogen in Endocytosing Macrophages Increases Severity of Pancreatitis in Mice. *Gastroenterology* 2018;154:704-718.e10.
 23. Qiu Y, Korteweg C, Chen Z, et al. Immunoglobulin G expression and its colocalization with complement proteins in papillary thyroid cancer. *Mod Pathol* 2012;25:36-45.
 24. Arora K, Chebib I, Zukerberg L, et al. Branched-chain in situ hybridization for κ and λ light chains: A powerful ancillary technique for determining B-cell clonality in cytology samples. *Cancer Cytopathol* 2016;124:203-12.
 25. Crespo ÂC, Mulik S, Dotiwala F, et al. Decidual NK Cells Transfer Granulysin to Selectively Kill Bacteria in Trophoblasts. *Cell* 2020;182:1125-1139.e18.
 26. Ng SS, De Labastida Rivera F, Yan J, et al. The NK cell granule protein NKG7 regulates cytotoxic granule exocytosis and inflammation. *Nat Immunol* 2020;21:1205-18.
 27. Halloran PF, Venner JM, Madill-Thomsen KS, et al. Review: The transcripts associated with organ allograft rejection. *Am J Transplant* 2018;18:785-95.
 28. Matsuo J, Douchi D, Myint K, et al. Iqgap3-Ras axis drives stem cell proliferation in the stomach corpus during homeostasis and repair. *Gut* 2021;70:1833-46.
 29. Pellin D, Loperfido M, Baricordi C, et al. A comprehensive single cell transcriptional landscape of human hematopoietic progenitors. *Nat Commun* 2019;10:2395.
 30. Scholl S, Bondeva T, Liu Y, et al. Additive effects of PI3-kinase and MAPK activities on NB4 cell granulocyte differentiation: potential role of phosphatidylinositol 3-kinase gamma. *J Cancer Res Clin Oncol* 2008;134:861-72.
 31. Koubourli DV, Yaparla A, Popovic M, et al. Amphibian (*Xenopus laevis*) Interleukin-8 (CXCL8): A Perspective on the Evolutionary Divergence of Granulocyte Chemotaxis. *Front Immunol* 2018;9:2058.
 32. Westin U, Lundberg E, Wihl JA, et al. The effect of immediate-hypersensitivity reactions on the level of SLPI, granulocyte elastase, alpha1-antitrypsin, and albumin in nasal secretions, by the method of unilateral antigen challenge. *Allergy* 1999;54:857-64.
 33. Guerra S, González JM, Climent N, et al. Selective induction of host genes by MVA-B, a candidate vaccine against HIV/AIDS. *J Virol* 2010;84:8141-52.
 34. Zeng Z, Liu H, Xu H, et al. Genome-wide association study identifies new loci associated with risk of HBV infection and disease progression. *BMC Med Genomics* 2021;14:84.
 35. Perros F, Hoogsteden HC, Coyle AJ, et al. Blockade of CCR4 in a humanized model of asthma reveals a critical role for DC-derived CCL17 and CCL22 in attracting Th2 cells and inducing airway inflammation. *Allergy* 2009;64:995-1002.
 36. Wilcock A, Bahri R, Bulfone-Paus S, et al. Mast cell disorders: From infancy to maturity. *Allergy* 2019;74:53-63.
 37. Magnúsdóttir EI, Grujic M, Roers A, et al. Mouse mast cells and mast cell proteases do not play a significant role in acute tissue injury pain induced by formalin. *Mol Pain* 2018;14:1744806918808161.
 38. Méndez-Enríquez E, Hallgren J. Mast Cells and Their Progenitors in Allergic Asthma. *Front Immunol* 2019;10:821.
 39. Garnache-Ottou F, Feuillard J, Ferrand C, et al. Extended diagnostic criteria for plasmacytoid dendritic cell leukaemia. *Br J Haematol* 2009;145:624-36.
 40. Collin M, Bigley V. Human dendritic cell subsets: an update. *Immunology* 2018;154:3-20.
 41. Zhang Z, Guo M, Li Y, et al. RNA-binding protein ZFP36/TTP protects against ferroptosis by regulating autophagy signaling pathway in hepatic stellate cells. *Autophagy* 2020;16:1482-505.
 42. Liu Y, Carson-Walter EB, Cooper A, et al. Vascular gene expression patterns are conserved in primary and metastatic brain tumors. *J Neurooncol* 2010;99:13-24.
 43. Gliga AR, Di Buccianico S, Åkerlund E, et al. Transcriptome Profiling and Toxicity Following Long-Term, Low Dose Exposure of Human Lung Cells to Ni and NiO Nanoparticles-Comparison with NiCl₂. *Nanomaterials (Basel)* 2020;10:649.
 44. Gharaie Fathabad S, Kurzhangen JT, Sadasivam M, et al. T

- Lymphocytes in Acute Kidney Injury and Repair. *Semin Nephrol* 2020;40:114-25.
45. Konno-Kumagai T, Fujishima F, Nakamura Y, et al. Programmed death-1 ligands and tumor infiltrating T lymphocytes in primary and lymph node metastasis of esophageal cancer patients. *Dis Esophagus* 2019;32:doi063.
 46. Roufas C, Georgakopoulos-Soares I, Zaravinos A. Molecular correlates of immune cytolytic subgroups in colorectal cancer by integrated genomics analysis. *NAR Cancer* 2021;3:zcab005.
 47. Pizzolato G, Kaminski H, Tosolini M, et al. Single-cell RNA sequencing unveils the shared and the distinct cytotoxic hallmarks of human TCRVδ1 and TCRVδ2 γδ T lymphocytes. *Proc Natl Acad Sci U S A* 2019;116:11906-15.
 48. Zhang L, Zhao Y, Dai Y, et al. Immune Landscape of Colorectal Cancer Tumor Microenvironment from Different Primary Tumor Location. *Front Immunol* 2018;9:1578.
 49. Schreiber TH, Wolf D, Boder M, et al. T cell costimulation by TNFR superfamily (TNFRSF)4 and TNFRSF25 in the context of vaccination. *J Immunol* 2012;189:3311-8.
 50. Delacher M, Imbusch CD, Hotz-Wagenblatt A, et al. Precursors for Nonlymphoid-Tissue Treg Cells Reside in Secondary Lymphoid Organs and Are Programmed by the Transcription Factor BATF. *Immunity* 2020;52:295-312. e11.
 51. Deng G, Song X, Fujimoto S, et al. Foxp3 Post-translational Modifications and Treg Suppressive Activity. *Front Immunol* 2019;10:2486.
 52. Xie M, Wei J, Xu J. Inducers, Attractors and Modulators of CD4⁺ Treg Cells in Non-Small-Cell Lung Cancer. *Front Immunol* 2020;11:676.
 53. Poch T, Krause J, Casar C, et al. Single-cell atlas of hepatic T cells reveals expansion of liver-resident naive-like CD4⁺ T cells in primary sclerosing cholangitis. *J Hepatol* 2021;75:414-23.
 54. Argyriou A, Wadsworth MH, Lendvai A, et al. Single cell sequencing reveals expanded cytotoxic CD4⁺ T cells and two states of peripheral helper T cells in synovial fluid of ACPA⁺ RA patients. *medRxiv* 2021. doi: <https://doi.org/10.1101/2021.05.28.21255902>
 55. Pasciuto E, Burton OT, Roca CP, et al. Microglia Require CD4 T Cells to Complete the Fetal-to-Adult Transition. *Cell* 2020;182:625-640.e24.
 56. Choi YS, Gullicksrud JA, Xing S, et al. LEF-1 and TCF-1 orchestrate T(FH) differentiation by regulating differentiation circuits upstream of the transcriptional repressor Bcl6. *Nat Immunol* 2015;16:980-90.
 57. Yashiro T, Takeuchi H, Kasakura K, et al. PU.1 regulates Ccr7 gene expression by binding to its promoter in naïve CD4⁺ T cells. *FEBS Open Bio* 2020;10:1115-21.
 58. Workel HH, Lubbers JM, Arnold R, et al. A Transcriptionally Distinct CXCL13+CD103+CD8⁺ T-cell Population Is Associated with B-cell Recruitment and Neoantigen Load in Human Cancer. *Cancer Immunol Res* 2019;7:784-96.
 59. Parsonage G, Machado LR, Hui JW, et al. CXCR6 and CCR5 localize T lymphocyte subsets in nasopharyngeal carcinoma. *Am J Pathol* 2012;180:1215-22.
 60. Zheng C, Zheng L, Yoo JK, et al. Landscape of Infiltrating T Cells in Liver Cancer Revealed by Single-Cell Sequencing. *Cell* 2017;169:1342-1356.e16.
 61. Vigne S, Chalmin F, Duc D, et al. IL-27-Induced Type 1 Regulatory T-Cells Produce Oxysterols that Constrain IL-10 Production. *Front Immunol* 2017;8:1184.
 62. Walsh DA, Borges da Silva H, Beura LK, et al. The Functional Requirement for CD69 in Establishment of Resident Memory CD8(+) T Cells Varies with Tissue Location. *J Immunol* 2019;203:946-55.
 63. Kong Y, Zhu L, Schell TD, et al. T-Cell Immunoglobulin and ITIM Domain (TIGIT) Associates with CD8⁺ T-Cell Exhaustion and Poor Clinical Outcome in AML Patients. *Clin Cancer Res* 2016;22:3057-66.
 64. Zheng Y, Rudensky AY. Foxp3 in control of the regulatory T cell lineage. *Nat Immunol* 2007;8:457-62.
 65. LeBien TW, Tedder TF. B lymphocytes: how they develop and function. *Blood* 2008;112:1570-80.
 66. Maddur MS, Sharma M, Hegde P, et al. Human B cells induce dendritic cell maturation and favour Th2 polarization by inducing OX-40 ligand. *Nat Commun* 2014;5:4092.
 67. Li Z, Ju X, Silveira PA, et al. CD83: Activation Marker for Antigen Presenting Cells and Its Therapeutic Potential. *Front Immunol* 2019;10:1312.
 68. Brinas F, Danger R, Brouard S. TCL1A, B Cell Regulation and Tolerance in Renal Transplantation. *Cells* 2021.
 69. Tedoldi S, Paterson JC, Cordell J, et al. Jaw1/LRMP, a germinal centre-associated marker for the immunohistological study of B-cell lymphomas. *J Pathol* 2006;209:454-63.
 70. Jaganjac M, Matijevic Glavan T, Zarkovic N. The Role of Acrolein and NADPH Oxidase in the Granulocyte-Mediated Growth-Inhibition of Tumor Cells. *Cells*

- 2019;8:292.
71. Halsey ES, Baldeviano GC, Edgel KA, et al. Symptoms and Immune Markers in Plasmodium/Dengue Virus Co-infection Compared with Mono-infection with Either in Peru. *PLoS Negl Trop Dis* 2016;10:e0004646.
 72. Sá VC, Silva TA, Reis CM, et al. The pattern of immune cell infiltration in chromoblastomycosis: involvement of macrophage inflammatory protein-1 alpha/CCL3 and fungi persistence. *Rev Inst Med Trop Sao Paulo* 2007;49:49-53.
 73. Ryckman C, Vandal K, Rouleau P, et al. Proinflammatory activities of S100: proteins S100A8, S100A9, and S100A8/A9 induce neutrophil chemotaxis and adhesion. *J Immunol* 2003;170:3233-42.
 74. Dias IH, Chapple IL, Milward M, et al. Sulforaphane restores cellular glutathione levels and reduces chronic periodontitis neutrophil hyperactivity in vitro. *PLoS One* 2013;8:e66407.
 75. Umansky V, Blattner C, Gebhardt C, et al. The Role of Myeloid-Derived Suppressor Cells (MDSC) in Cancer Progression. *Vaccines (Basel)* 2016.
 76. Srikrishna G. S100A8 and S100A9: new insights into their roles in malignancy. *J Innate Immun* 2012;4:31-40.
 77. Wu SY, Fu T, Jiang YZ, et al. Natural killer cells in cancer biology and therapy. *Mol Cancer* 2020;19:120.
 78. Ebrahimi Meimand S, Rostam-Abadi Y, Rezaei N. Autism spectrum disorders and natural killer cells: a review on pathogenesis and treatment. *Expert Rev Clin Immunol* 2021;17:27-35.
 79. Liu C, Gong Y, Zhang H, et al. Delineating spatiotemporal and hierarchical development of human fetal innate lymphoid cells. *Cell Res* 2021;31:1106-22.
 80. Hidalgo LG, Sis B, Sellares J, et al. NK cell transcripts and NK cells in kidney biopsies from patients with donor-specific antibodies: evidence for NK cell involvement in antibody-mediated rejection. *Am J Transplant* 2010;10:1812-22.
 81. Moesta AK, Parham P. Diverse functionality among human NK cell receptors for the C1 epitope of HLA-C: KIR2DS2, KIR2DL2, and KIR2DL3. *Front Immunol* 2012;3:336.
 82. Deniger DC, Maiti SN, Mi T, et al. Activating and propagating polyclonal gamma delta T cells with broad specificity for malignancies. *Clin Cancer Res* 2014;20:5708-19.
 83. Märklin M, Hagelstein I, Koerner SP, et al. Bispecific NKG2D-CD3 and NKG2D-CD16 fusion proteins for induction of NK and T cell reactivity against acute myeloid leukemia. *J Immunother Cancer* 2019;7:143.
 84. Wu K, Lin K, Li X, et al. Redefining Tumor-Associated Macrophage Subpopulations and Functions in the Tumor Microenvironment. *Front Immunol* 2020;11:1731.
 85. Oreja-Guevara C, Ramos-Cejudo J, Aroeira LS, et al. TH1/TH2 Cytokine profile in relapsing-remitting multiple sclerosis patients treated with Glatiramer acetate or Natalizumab. *BMC Neurol* 2012;12:95.
 86. Pernet I, Reymermier C, Guezennec A, et al. Calcium triggers beta-defensin (hBD-2 and hBD-3) and chemokine macrophage inflammatory protein-3 alpha (MIP-3alpha/CCL20) expression in monolayers of activated human keratinocytes. *Exp Dermatol* 2003;12:755-60.
 87. Carlucci F, Ishaque A, Ling GS, et al. C1q Modulates the Response to TLR7 Stimulation by Pristane-Primed Macrophages: Implications for Pristane-Induced Lupus. *J Immunol* 2016;196:1488-94.
 88. Werb Z, Chin JR. Apoprotein E is synthesized and secreted by resident and thioglycollate-elicited macrophages but not by pyran copolymer- or bacillus Calmette-Guerin-activated macrophages. *J Exp Med* 1983;158:1272-93.
 89. Tang J, Shi Y, Zhan L, et al. Downregulation of GPR183 on infection restricts the early infection and intracellular replication of mycobacterium tuberculosis in macrophage. *Microb Pathog* 2020;145:104234.
 90. Bus P, Pierneef L, Bor R, et al. Apolipoprotein C-I plays a role in the pathogenesis of glomerulosclerosis. *J Pathol* 2017;241:589-99.
 91. Chen J, Yao Y, Gong C, et al. CCL18 from tumor-associated macrophages promotes breast cancer metastasis via PITPNM3. *Cancer Cell* 2011;19:541-55.
 92. Workman MJ, Troisi E, Targan SR, et al. Modeling Intestinal Epithelial Response to Interferon- γ in Induced Pluripotent Stem Cell-Derived Human Intestinal Organoids. *Int J Mol Sci* 2020;22:288.
 93. Deng W, Su Z, Liang P, et al. Single-cell immune checkpoint landscape of PBMCs stimulated with *Candida albicans*. *Emerg Microbes Infect* 2021;10:1272-83.
 94. Lin C, He H, Liu H, et al. Tumour-associated macrophages-derived CXCL8 determines immune evasion through autonomous PD-L1 expression in gastric cancer. *Gut* 2019;68:1764-73.
 95. Kim HR, Lee HS, Lee KS, et al. An Essential Role for TAGLN2 in Phagocytosis of Lipopolysaccharide-activated Macrophages. *Sci Rep* 2017;7:8731.
 96. Hinshaw DC, Shevde LA. The Tumor Microenvironment Innately Modulates Cancer Progression. *Cancer Res* 2019;79:4557-66.

97. Nabeki B, Ishigami S, Uchikado Y, et al. Interleukin-32 expression and Treg infiltration in esophageal squamous cell carcinoma. *Anticancer Res* 2015;35:2941-7.
98. Tanaka A, Sakaguchi S. Regulatory T cells in cancer immunotherapy. *Cell Res* 2017;27:109-18.
99. Ling Y, Fan L, Dong C, et al. Combined influence of adjuvant therapy and interval after surgery on peripheral CD4(+) T lymphocytes in patients with esophageal squamous cell carcinoma. *Exp Ther Med* 2010;1:113-20.
100. Wang SS, Liu W, Ly D, et al. Tumor-infiltrating B cells: their role and application in anti-tumor immunity in lung cancer. *Cell Mol Immunol* 2019;16:6-18.
101. Vasyutina E, Boucas JM, Bloehdorn J, et al. The regulatory interaction of EVI1 with the TCL1A oncogene impacts cell survival and clinical outcome in CLL. *Leukemia* 2015;29:2003-14.
102. Li H, Yan X, Liu L, et al. T-cell leukemia/lymphoma-1A predicts the clinical outcome for patients with stage II/III colorectal cancer. *Biomed Pharmacother* 2017;88:924-30.
103. Oberbeck S, Schrader A, Warner K, et al. Noncanonical effector functions of the T-memory-like T-PLL cell are shaped by cooperative TCL1A and TCR signaling. *Blood* 2020;136:2786-802.
104. Song KH, Oh SJ, Kim S, et al. HSP90A inhibition promotes anti-tumor immunity by reversing multi-modal resistance and stem-like property of immune-refractory tumors. *Nat Commun* 2020;11:562.
105. Zhang S, Tian R, Bei C, et al. Down-Regulated CMTM2 Promotes Epithelial-Mesenchymal Transition in Hepatocellular Carcinoma. *Onco Targets Ther* 2020;13:5731-41.
106. Ngambenjawong C, Gustafson HH, Pun SH. Progress in tumor-associated macrophage (TAM)-targeted therapeutics. *Adv Drug Deliv Rev* 2017;114:206-21.
107. Ohta M, Kitadai Y, Tanaka S, et al. Monocyte chemoattractant protein-1 expression correlates with macrophage infiltration and tumor vascularity in human esophageal squamous cell carcinomas. *Int J Cancer* 2002;102:220-4.
108. Nakajima S, Mimura K, Saito K, et al. Neoadjuvant Chemotherapy Induces IL34 Signaling and Promotes Chemoresistance via Tumor-Associated Macrophage Polarization in Esophageal Squamous Cell Carcinoma. *Mol Cancer Res* 2021;19:1085-95.
109. Urakawa N, Utsunomiya S, Nishio M, et al. GDF15 derived from both tumor-associated macrophages and esophageal squamous cell carcinomas contributes to tumor progression via Akt and Erk pathways. *Lab Invest* 2015;95:491-503.
110. Kodama T, Koma YI, Arai N, et al. CCL3-CCR5 axis contributes to progression of esophageal squamous cell carcinoma by promoting cell migration and invasion via Akt and ERK pathways. *Lab Invest* 2020;100:1140-57.
111. Haque ASMR, Moriyama M, Kubota K, et al. CD206(+) tumor-associated macrophages promote proliferation and invasion in oral squamous cell carcinoma via EGF production. *Sci Rep* 2019;9:14611.
112. Wang Y, Tong X, Zhang J, et al. The complement C1qA enhances retinoic acid-inducible gene-I-mediated immune signalling. *Immunology* 2012;136:78-85.
113. Chen LH, Liu JF, Lu Y, et al. Complement C1q (C1qA, C1qB, and C1qC) May Be a Potential Prognostic Factor and an Index of Tumor Microenvironment Remodeling in Osteosarcoma. *Front Oncol* 2021;11:642144.
114. Logtenberg MEW, Scheeren FA, Schumacher TN. The CD47-SIRPα Immune Checkpoint. *Immunity* 2020;52:742-52.
115. Roumenina LT, Daugan MV, Noé R, et al. Tumor Cells Hijack Macrophage-Produced Complement C1q to Promote Tumor Growth. *Cancer Immunol Res* 2019;7:1091-105.

Cite this article as: Zheng F, Zhang W, Yang B, Chen M. Multi-omics profiling identifies C1QA/B⁺ macrophages with multiple immune checkpoints associated with esophageal squamous cell carcinoma (ESCC) liver metastasis. *Ann Transl Med* 2022;10(22):1249. doi: 10.21037/atm-22-5351

Table S1 List of antibodies for multiplex immunohistofluorescence assay

Antibodies	Source	Identifier
CD3	Cell signaling technology	Cat#: 85061s
CD11b	Abcam	Cat#: ab13357
Pan cytokeratin	BioLegend	Cat#: 914704
CD68	BioLegend	Cat#: 916104
CD138	Invitrogen	Cat#: 362900
CD4	Abcam	Cat#: ab133616
CD8	BioLegend	Cat#: 372902
CD69	Abcam	Cat#: ab234511
Foxp3	Cell Signaling Technology	Cat#: 12653s
CD57	BD	Cat#: 555618
Ki67	BD	Cat#: 556609
GAMMADELTA	Novus Biologicals	Cat#: NBP2-62225